Council on Tall Buildings and Urban Habitat
CTBUH Research Paper
ctbuh.org/papers

Title: **Validation of the Aerodynamic Model Method**

Author: Daryl W. Boggs, Cermak Peterka Petersen (CPP), Inc.

Subject: Wind Engineering

Publication Date: 1992

Original Publication: Journal of Wind Engineering and Industrial Aerodynamics 1992

Paper Type:

1. **Book chapter/Part chapter**
2. Journal paper
3. Conference proceeding
4. Unpublished conference paper
5. Magazine article
6. Unpublished

© Council on Tall Buildings and Urban Habitat / Daryl W. Boggs

Journal of Wind Engineering and Industrial Aerodynamics, 41 – 44(1992) 1011 – 1022
Elsevier

Validation of the Aerodynamic Model Method

D.W. Boggs

Cermak Peterka Petersen, Inc., 1415 Blue Spruce Drive, Ft. Collins, CO 80524

Abstract

The principles of aeroelastic and aerodynamic models are distinguished, and aeroelastic magnification is identified as a possible source of unacceptable error in the latter type of model. Past justifications of aerodynamic modeling have not clearly identified the relevant error-controlling parameters, or have not established quantitative limits required for valid results on the parameters studied. Results of new tests show that the reduced velocity, in conjunction with the mass-damping parameter, provides a good characterization of the aeroelastic magnification factor for an 8:1:1 square cylinder in a simulated suburban environment.

AEROELASTIC AND AERODYNAMIC MODELS

The wind response of a tall building vibrating in a natural mode is described by

$$m^*\ddot{\xi} + c^*\dot{\xi} + k^*\xi = P^* \tag{1}$$

where m^*, c^*, k^*, and P^* are the generalized mass, damping coefficient, stiffness, and load;

$$P^* = \sum_i P_i \phi_i \tag{2}$$

where P_i is the external or *aerodynamic* load acting at floor i, and ϕ_i is the modal deflection at floor i. The actual deflections are $\delta_i = \xi\phi_i$. In general the load may be dependent on the structure's response, so the generalized load must be written $P^* = P^*(t, \xi, \dot{\xi}, \ddot{\xi})$. The presence of ξ and its derivatives on the right side of (1) represents aeroelastic feedback, rendering the equation nonlinear. In the traditional *aeroelastic* test, a scale model is tuned to the dynamic characteristics corresponding to the left side of (1), and placed in a boundary-layer wind tunnel simulating the wind environment required by the right side. The model is then a complete analog of Eq. (1), and the response $\xi(t)$ can be observed directly. The generalized aerodynamic load, P^*, exists but is not measured.

Recently the aeroelastic model has, for practical purposes, been replaced by a model type having negligible displacement response and on which the generalized aerodynamic load can be measured. This is defined herein as an *aerodynamic* model. Various types are used, based on

either force balance or pressure measurements, the latter of which requires the simultaneous sensing of perhaps hundreds of transducers. In any case P^* is measured, and from this the response is computed as, for example,

$$\tilde{\mathbf{P}}^{*2} = \int_{\infty}^{0} |H(f)|^2 S_{P^*}(f)\,df \tag{3}$$

where $\mathbf{P}^* = \Sigma \mathbf{P}_i \phi_i$ is the *generalized response*, and $\mathbf{P}_i$ is the internal or static-equivalent load at floor i. The structure's damping and natural frequency are incorporated in the mechanical admittance, $|H(f)|^2 = 1/\{[1-(f/f_0)^2]^2 + (2\zeta f/f_0)^2\}$ In the simplest and most popular form of aerodynamic model, a "high-frequency base balance" is used to measure the base moment $M(t)$, which is transformed to a mean-square spectral density $S_M(f)$, from which the mean square response (i.e. static equivalent) base moment is computed according to

$$\tilde{\mathbf{M}}^2 = \int_0^{\infty} |H(f)|^2 S_M(f)\,df \tag{4}$$

This works (approximately) for most tall structures because the mode shape is nearly a straight line, e.g. $\phi_i = z_i$, in which case P^* and $\mathbf{P}^*$ reduce to M and $\mathbf{M}$, respectively.

There are three major obstacles to performing and accepting the aerodynamic method. First, it must be assumed that there is no aeroelastic feedback; i.e. the aerodynamic load P^* is a function of time only. Second, it must be assumed that the mode shape in sway is linear; for the torsional component the mode shape must be constant. Finally, there is the practical problem of building and implementing such a balance.

The third obstacle has been solved through balance design which achieves a high stiffness/strain ratio, to obtain a high signal level and high natural frequency. This is invariably a custom piece of equipment which further requires specialized installation, instrumentation, and data collection/analysis procedures. These issues are discussed in some detail in references 1 and 2.

The second obstacle has been addressed by correction factors to account for real mode shapes which deviate from ideal [3,4,5,6]. Corrections as large as 50 percent are often stated; however, these factors are sometimes misused and give a misleading account of the real uncertainty introduced by nonideal mode shapes, due to arbitrary normalization or scaling of the shapes. The typical overall uncertainty in Eq. (4) is actually less than 5 percent in sway and 10 to 20 percent in torsion [6].

Little quantitative information is available on the first problem, although it is generally assumed that ignoring aeroelastic effects is slightly conservative. It is well known, however, that under certain conditions, e.g. vortex shedding or galloping, an aerodynamic model would give unacceptable, unconservative results. This problem is commonly simplified and described in terms of *aerodynamic* damping, or motion-induced force working in conjunction with the structural damping. Positive aerodynamic damping increases the total damping, thus decreasing the response. For usual buildings and winds the aerodynamic damping is small and positive, and is therefore commonly neglected. For crosswind loading, however, it may be negative and large

for high wind speeds or large building displacements. This causes large aeroelastic magnification, invalidating the response which would be calculated from an aerodynamic model.

The remainder of this paper, therefore, is concerned with aeroelastic magnification of response in the crosswind direction.

PREVIOUS VALIDATION EFFORTS

A number of researchers [2,7,8,9] have demonstrated conditions for both valid and invalid aerodynamic results for specific cases by comparing the results of aeroelastic and aerodynamic models of the same building. Although these studies have been vital in establishing the general level of acceptance which the aerodynamic method now enjoys, they have not provided quantitative or general limits on conditions for validity. Indeed, even the parameters of most significance have not been agreed upon. It may be stated, for example, that sufficient (but not necessary) conditions are that the reduced velocity be less than the critical value for vortex shedding, while others may demonstrate valid results provided the rms tip displacement (effected by varying the damping) is below some (possibly vague) critical value. Other parameters, such as building density, building shape, and boundary-layer characteristics, have not been studied systematically.

Further, the validation efforts have been interpreted from a research viewpoint as opposed to standard practice. Discrepancies between aeroelastic and aerodynamic results as high as 40 percent have commonly been accepted as valid, even though such an error would not be acceptable to most structural engineers. The discrepancies in reported results to date are due to a combination of aeroelastic effects, experimental error, and improper or simplified data analysis (such as the use of a white-noise approximation in place of Eq. (3)). These studies are considered in detail in Reference 1.

PRESENT VALIDATION TESTS

Tests were performed in the boundary layer wind tunnel shown in Fig. 1. The wind profile, representative of a suburban environment, is shown in Fig. 2. Analysis of the length scale of longitudinal turbulence showed that the model scale could range from 1:200 to 1:500 depending on test speed, elevation of significance, and assumed atmospheric properties. The model building, $H \times D \times D = 24 \times 3 \times 3$ in., then represents prototype buildings 400 to 1000 ft tall.

The aerodynamic model and balance setup is shown in Fig. 3. The balance is described in detail in Reference 1. The building models were constructed of 0.125-in.-thick balsa as shown, and supported on the balance by a thin-wall steel tube sting. Dynamic performance is indicated by the total admittance of the balance, model, and filters in Fig. 4, and by the impulse response in Fig. 6. In terms of absolute frequency the bandwidth is about 90 Hz ±1 dB. Tests were conducted at a reference speed $U = \overline{u}_H = 30$ fps. Using this and the reference width $D = 0.25$ ft, the bandwidth in reduced frequency is 0.7, corresponding to a minimum reduced velocity of 1.4. The small ±1 dB variation was corrected in the measured PSD's.

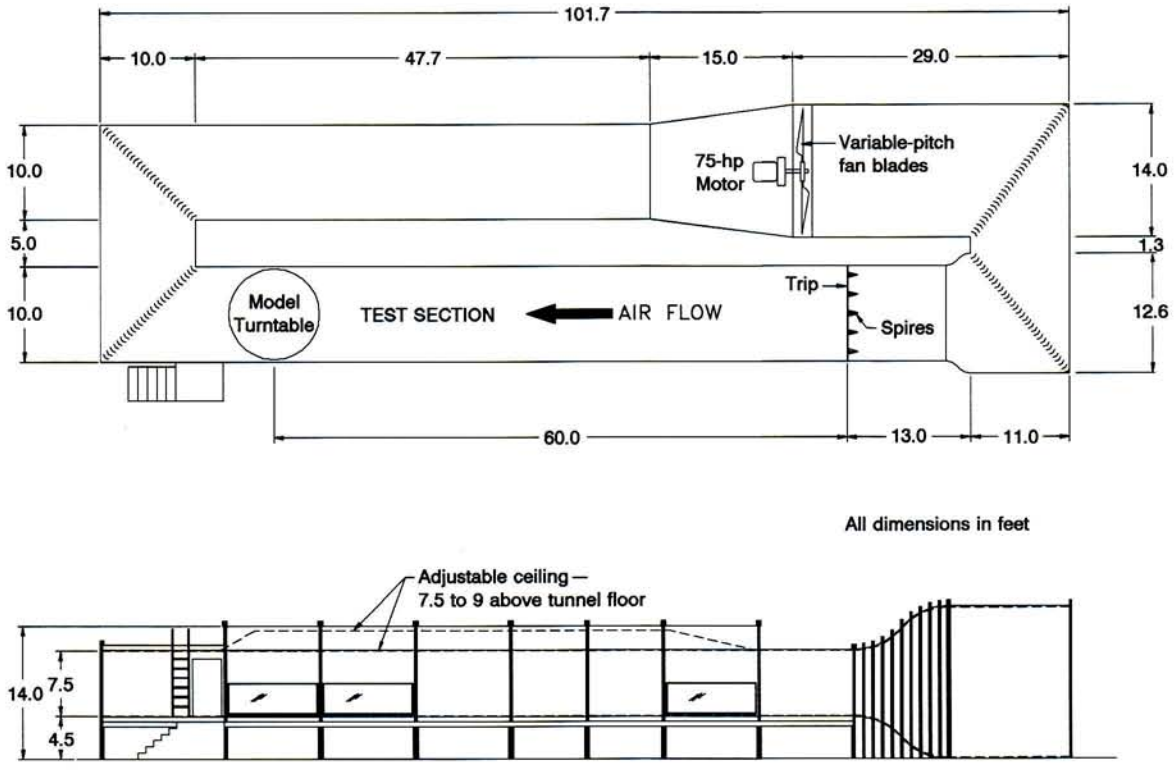

Figure 1. Closed-circuit boundary-layer wind tunnel, wind engineering laboratory, Cermak Peterka Petersen Inc.

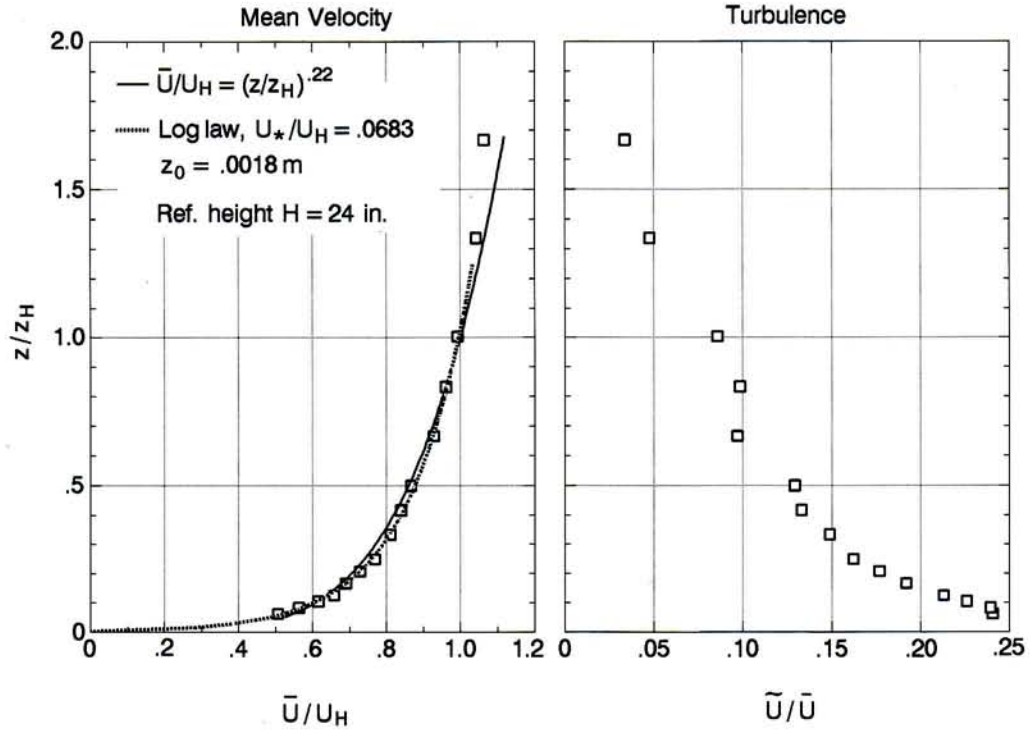

Figure 2. Boundary layer profiles measured in wind tunnel for aeroelastic and aerodynamic model tests on square cylinders.

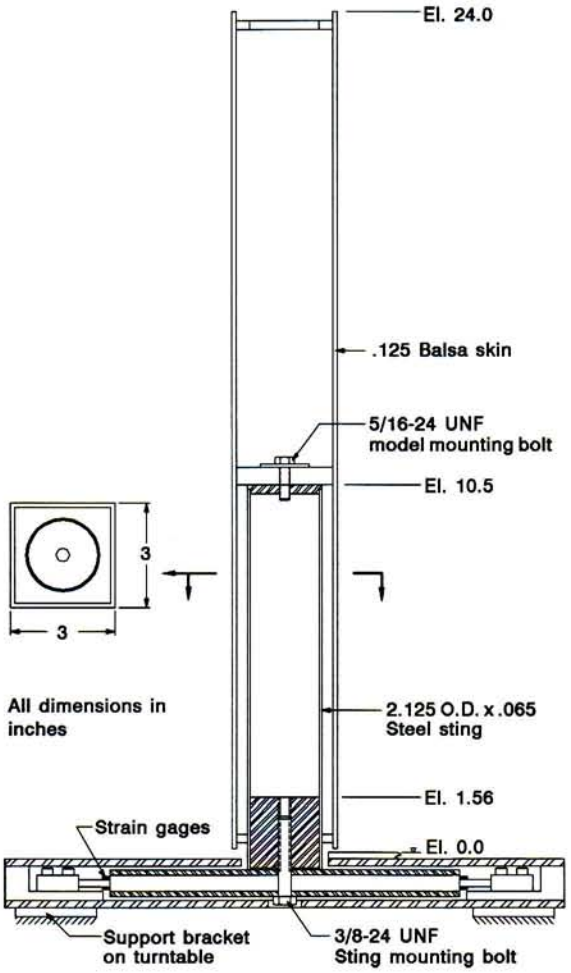

Figure 3. Aerodynamic balance and model.

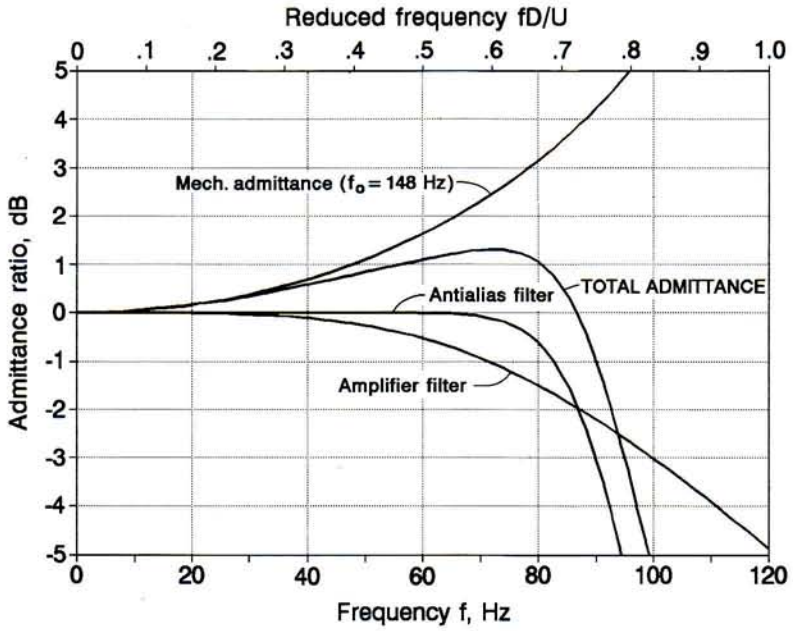

Figure 4. Transfer function of the aerodynamic balance and instrument system.

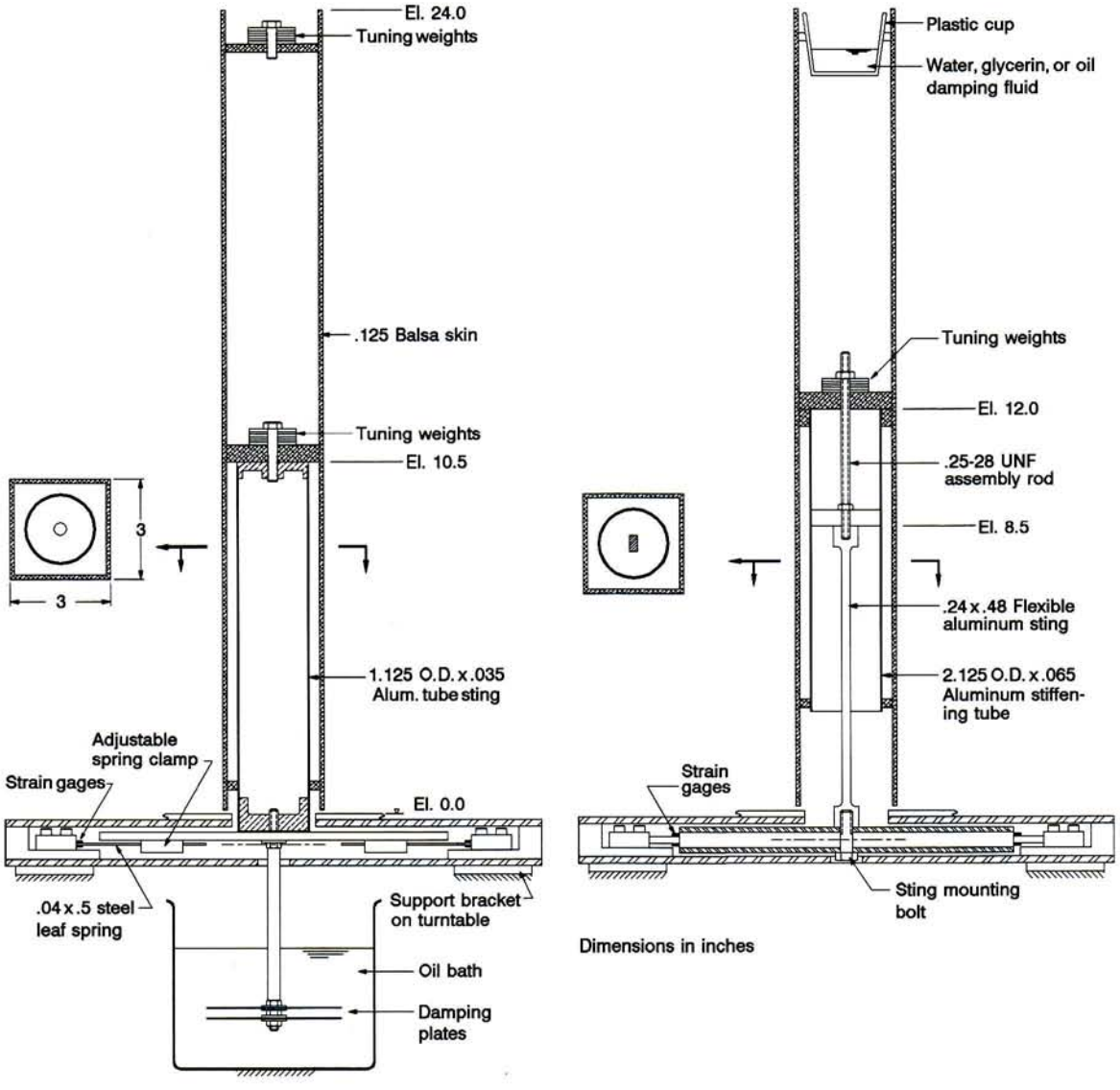

Figure 5. (*a*) Universal-type aeroelastic balance. (*b*) Flexible-sting aeroelastic balance.

Two aeroelastic model and balance systems were used, shown in Fig. 5. In the "universal" aeroelastic balance, (*a*), the tube sting is bolted rigidly to a flat plate which is in turn supported from a heavy inertial frame by thin steel leaf springs. The spring clamps are adjustable and the springs can be replaced with matched pairs of various thicknesses to obtain a wide range of model stiffness. Damping is provided by the shearing action of a plate vibrating horizontally in a viscous fluid. Although this system has been used successfully in a number of model tests, it may become nonlinear under the large amplitude responses required here, and some of the results were discarded. The second aeroelastic balance, (*b*), is based on the aerodynamic balance which, because of its very high inherent stiffness, had a load capacity and signal output easily capable of handling the large loads produced by an aeroelastic model. Aeroelastic flexure was provided by the 0.24×0.48×8-in. long aluminum bar.

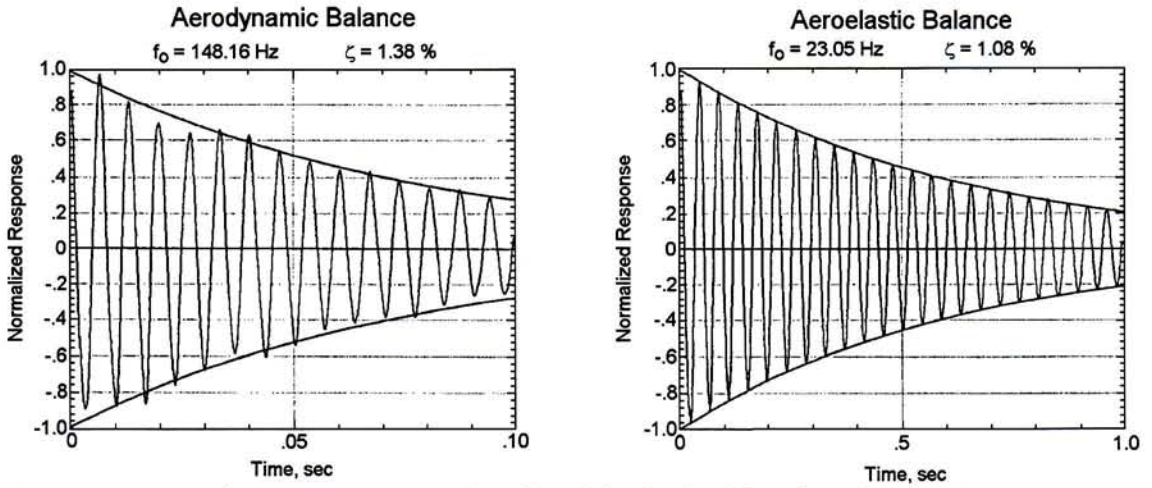

Figure 6. Natural frequency and damping of models obtained from impulse response.

The test wind speed was limited from about 15 fps at the low end—below which signal/noise effects and Reynolds no. scaling effects produced anomalous results—to about 46 fps on the high end—as limited by the wind-tunnel fan. It was desired to obtain test results over a range of reduced velocity greater than this 3:1 ratio. This was achieved by testing each mass configuration of the model in at least two stiffness ranges. This proved to be particularly convenient in the second balance setup, where rotating the balance 90 degrees resulted in a four-fold change in stiffness, i.e. a two-fold change in natural frequency—and therefore reduced velocity—for a given test speed.

Proper aeroelastic modeling requires identification of the model's generalized mass, natural frequency, and damping. For the rigid, pivoting-type models used here, the generalized mass is the moment of inertia about the center of rotation. This was determined indirectly by measuring the model's rotational stiffness during static calibration and the natural frequency under free vibration. The latter is easily measured, along with the damping ratio, by a simple pluck test, of which a representative trace is shown in Fig. 6.

It is in this respect that each of the aeroelastic balance systems has its own disadvantage. In the first system, nonlinear stiffness makes it difficult to determine the moment of inertia indirectly, as it *appears* to be amplitude-dependent. In the second system, the center of rotation is not well defined and depends on the effective height of load application, which in turn depends primarily on the mass distribution within the model. Care was taken to perform the static calibration with loads applied at the proper height, and to add or remove tuning weights at the proper height also. Fortunately, the theoretical center of rotation can be calculated without difficulty, and the dynamic center of rotation under large amplitudes can be observed directly (although not precisely) under high winds. Unfortunately these are not identical due to uncertainties in component flexibilities, mass distribution, and the effective height of the externally applied load.

Conditioners for strain gage bridge networks from the model balances provided gage excitation, amplification, and 2-pole Butterworth low-pass filtering at 100 Hz and 16 dB/octave.

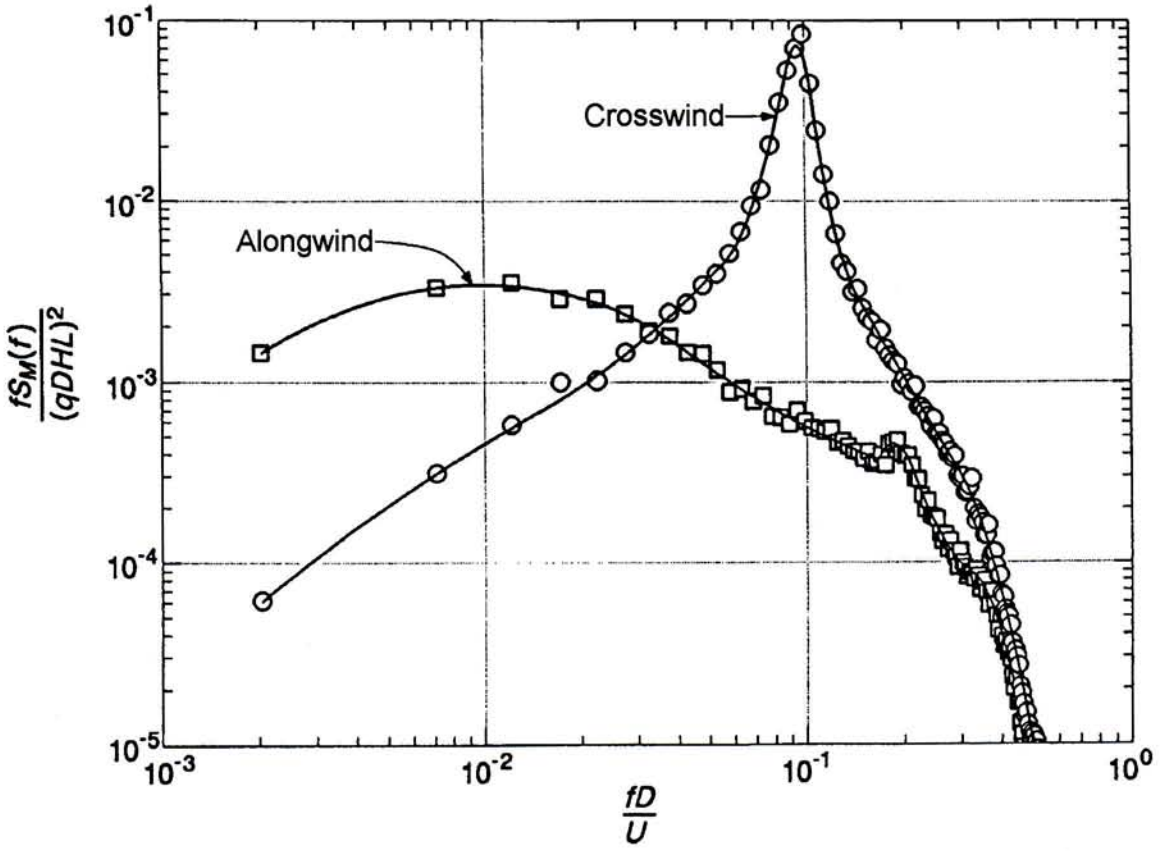

Figure 7. Power spectral densities of base moment from aerodynamic model.

Additional antialias filters provided 6-pole Butterworth low-pass filtering at 48 dB/octave and a cutoff frequency adjusted to maximize the total system bandwidth in the aerodynamic model (Fig. 4). A Pitot-static tube was used to measure the reference speed $U = \overline{u}_H$ and pressure $q = \rho U^2/2$, where ρ is the laboratory air density. Filtered balance and transducer signals were collected using a Metrabyte Dash-16 A/D converter in an IBM PC-AT computer. For the PSD calculations, a 16-bit integer FFT was performed by an Ariel PC-FFT hardware option in the host computer, and the PSD was completed using 32-bit real arithmetic. Thirty-two data segments of 2048 samples per channel each were averaged to decrease the random error associated with PSD measurements.

DATA REDUCTION

Power spectral densities were computed from the aerodynamic model base moment, and B-splines were fit to the resulting data points. These results are shown in Fig. 7. Note that the crosswind component shows a distinct critical value for vortex shedding at a reduced frequency (velocity) of 0.095 (10.5). The predicted rms base moment response coefficient was then computed for hypothetical structures having various natural frequencies and damping ratios using

a nondimensional version of Eq. (4), based on a reference moment $qDHL$, L = length from model tip to center of rotation:

$$(\tilde{C}_{\mathbf{M}})_{\text{pred}} \equiv \frac{\tilde{\mathbf{M}}}{qDHL} = \sqrt{\int_0^{(fD/U)_{\max}} |H(fD/U)|^2 \frac{fS_M(fD/U)}{(qDHL)^2} d(\ln fD/U)} \tag{5}$$

To perform this integration, the upper frequency limit was set at about 0.5, and Simpson's rule was utilized except for a narrow band at $f_0D/U \pm 1$ percent. The contribution of this band was computed by assuming a constant spectral value and utilizing a closed-form solution for response to band-limited white noise [1]. An alternative commonly used approximation for the response which involves the complete white-noise approximation,

$$\tilde{\mathbf{M}}^2 = \frac{\pi}{4\zeta} f_0 S_M(f_0) + \tilde{M}^2 \tag{6}$$

was avoided because it leads to errors of 10 to 20 percent in the rms response [1].

In the aeroelastic models, $\tilde{\mathbf{M}}$ was measured directly by the balance. In both model types this value is initially referenced to the center of action of the balances, about 1 model inch below ground. In all cases, mode-shape adjustments were made [6] so that the values reported herein pertain to ground level, with an idealized rigid-body model pivoting about ground elevation.

Displacements were not measured directly. For both the aerodynamic and aeroelastic values the normalized rms tip displacement, $\tilde{\delta}/D$, was computed from $\tilde{\mathbf{M}}$ according to

$$\frac{\tilde{\delta}}{D} = \frac{3}{8\pi^2}\left(\frac{\rho D^2 HL^2}{3J}\right)\left(\frac{U}{f_0 D}\right)^2 \tilde{C}_{\mathbf{M}} \tag{7}$$

where ρ = air density and L = length from tip to center of rotation. The first term in parentheses is the reciprocal of the mass ratio, defined by the ratio of the generalized mass J to the moment of inertia of displaced air. Finally, the predicted and observed results were compared by computing an *aeroelastic magnification factor*, defined as

$$\text{AMF} = \frac{(\tilde{C}_{\mathbf{M}})_{\text{obs}}}{(\tilde{C}_{\mathbf{M}})_{\text{pred}}} = \frac{(\tilde{\delta}/D)_{\text{obs}}}{(\tilde{\delta}/D)_{\text{pred}}} \tag{8}$$

RESULTS

Figure 8 shows aerodynamic (predicted) and aeroelastic (observed) values for two representative damping ratios and several mass ratios. The data are plotted in three ways: first as moment coefficient, in which case the predicted aerodynamic results are independent of mass ratio and is therefore concise; second as normalized tip deflection, which is the form most often observed in literature [2][7][8][9] and from which one may test the contention that displacement is a key parameter defining validity; finally as the Aeroelastic Magnification Factor, to facilitate numerical evaluation of the error. It is readily observed that the error may become quite large as U/f_0D exceeds the critical value for vortex shedding, especially for the lower mass ratios and damping.

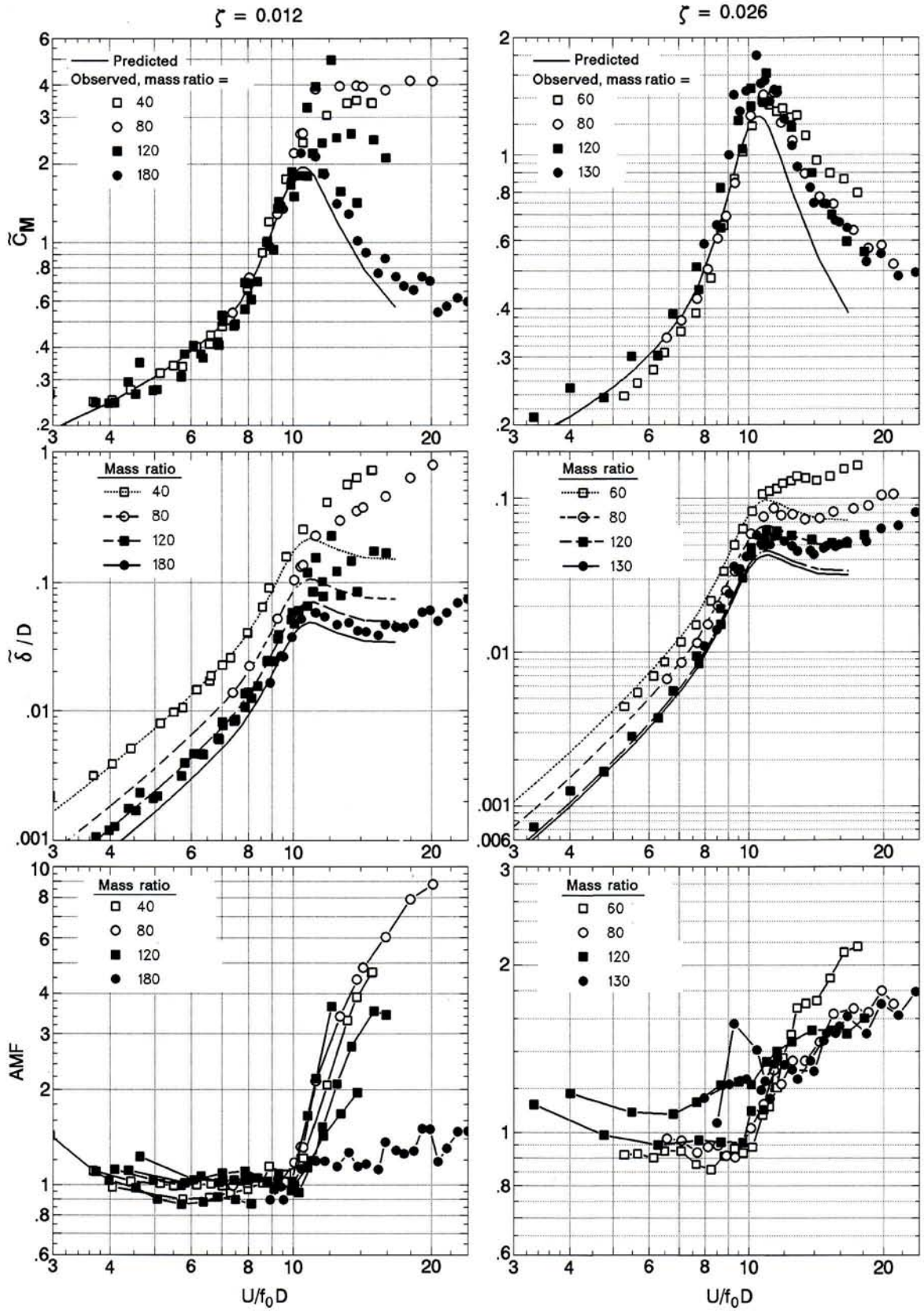

Figure 8. Predicted and observed response as function of reduced velocity for two damping values.

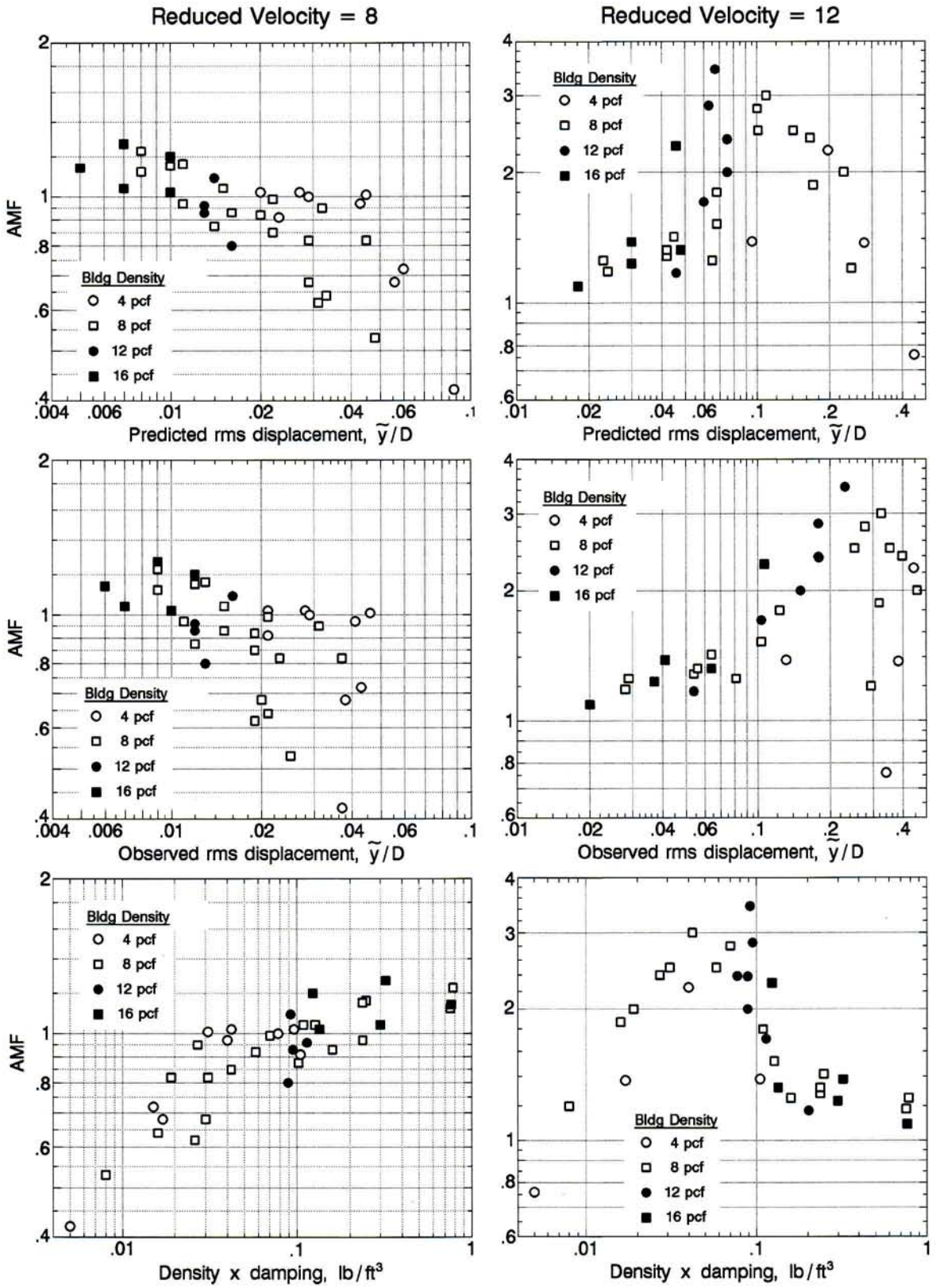

Figure 9. AMF as function of various parameters at reduced velocity 8 and 12.

The complete series of tests included mass ratios ranging from 40 to 220 (corresponding to densities from about 3 to 16 lb/ft^3), damping ratios from 0.002 to 0.084, and reduced velocities from about 3 to 20. Figure 9 shows results from all tests at two representative values of reduced velocity, plotted as the AMF vs. various parameters, in an attempt to ascertain the parameter best describing the error, i.e. producing the least scatter. The parameters include the normalized rms tip displacement, both as predicted by the aerodynamic model and as observed on the aeroelastic model, and the product of density and damping, $\gamma\zeta$. The density is defined as the product of mass ratio and the density of air at standard conditions:

$$\gamma = \frac{3J}{D^2 HL^2} \frac{\rho_{std}}{\rho} g \tag{9}$$

For a fixed building size as used here, $\gamma\zeta$ is proportional to $4\pi m\zeta/(\rho D^2)$, variously known as "reduced damping" or the Scruton no. It is readily apparent that this parameter is superior to the first two in defining a functional relationship with the AMF. At each reduced velocity a smooth curve was drawn through the data points of AMF vs. $\gamma\zeta$ to yield the family of curves shown in Fig. 10. The Scruton no. as used here is defined as

$$Sc = 4\pi\zeta \frac{J}{\rho D^2 HL^2 / 3} \tag{10}$$

The following observations are made:

- The AMF is not a monotonic function of *Sc*. Valid results can be obtained for either high or low values; a large AMF may occur for intermediate values.

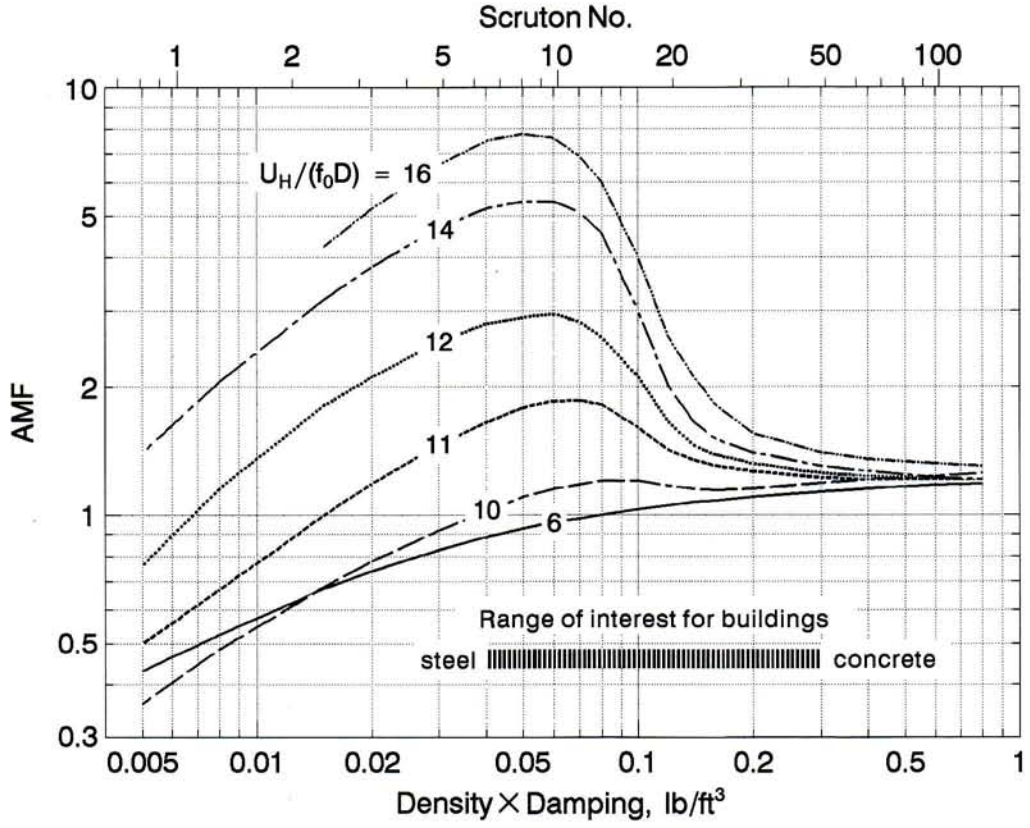

Figure 10. Aeroelastic Magnification Factor as a function of mass-damping parameter.

- Valid results occur for most buildings for subcritical reduced velocity (10.5 for this case). For low-density lightly damped buildings the AMF becomes large when the reduced velocity exceeds the critical vortex-shedding value. For many buildings the AMF never exceeds 1.2.
- The normalized rms tip deflection appears to be a poor indicator of aeroelastic magnification, and the existence of a critical value $(\widetilde{\delta}/D)_{cr} = 0.025$, as hypothesized in [8] and often accepted [10][11], is not justified. In Fig. 9 for example, at $U/f_0D = 8$ the AMF never exceeds about 1.2 and actually *decreases* for *increasing* normalized displacement; at $U/f_0D = 12$ the AMF is modest until a threshold at about $\widetilde{\delta}/D \approx 0.1$.

CONCLUSION

These results present a clear picture of the consequences of neglecting aeroelastic feedback and define conditions when an aerodynamic model is valid. Ideally these tests should be repeated for other body shapes and boundary layers. Although the results apply quantitatively only to a slender square building in a suburban boundary layer, qualitative observations can be expected to apply more generally. Most important is the significant role played by the Scruton no., which appears to be a better indicator of aeroelastic amplification than is the often-assumed rms tip displacement.

References

1. Boggs, Daryl W., "Wind Loading and Response of Tall Structures using Aerodynamic Models," Ph.D. Dissertation, Colorado State University, 1991.
2. Tschanz, Tony, "Measurement of Total Dynamic Loads using Elastic Models with High Natural Frequencies," *Wind Tunnel Modeling for Civil Engineering Applications*, pp. 296 – 312.
3. Tallin, A., and Ellingwood, B., "Analysis of Torsional Moments on Tall Buildings," *Jl Wind Engrg Ind Aero*, 18(1985) 191 – 195.
4. Vickery, P.J. et al., "The Effect of Mode Shape on the Wind-Induced Response of Tall Buildings," *Proc. Fifth U.S. National Conference on Wind Engineering*, 1985, pp. 1B-41 – 1B-48.
5. Holmes, J.D., "Mode Shape Corrections for Dynamic Response to Wind," *Engrg Struct* 9(1987) 210 – 212.
6. Boggs, Daryl W., and Peterka, Jon A., "Aerodynamic Model Tests of Tall Buildings," *Jl Engrg Mech*, ASCE, Vol. 115, No. 3, March, 1989, pp. 618 – 635.
7. Reinhold, T.A., and Sparks, P.R., "The Influence of Wind Direction on the Response of a Square-Section Tall Building," *Wind Engineering* (Proceedings of the Fifth International Conference), ed. J.E. Cermak, Pergamon Press, 1979, pp. 685 – 698.
8. Kwok, K.C.S., and Melbourne, W.H., "Wind-Induced Lock-In Excitation of Tall Structures," *Jl Struct Div*, ASCE, Vol. 107, No. ST1, January, 1981, pp. 57 – 72.
9. Kareem, A., "Acrosswind Response of Buildings," *Jl Struct Div*, ASCE, Vol. 108, No. ST4, April, 1982, pp. 869 – 887.
10. Simiu, Emil, "Modern Developments in Wind Engineering: Part 4," *Engrg Struct*, Vol. 5, October, 1983, pp. 273 – 281.
11. Simiu, Emil, and Scanlan, Robert H., *Wind Effects on Structures: An Introduction to Wind Engineering* (2nd ed.), John Wiley & Sons, New York, 1986, p. 312.